Behavior of High Strength Fiber-Reinforced Concrete beams under cyclic loading

Laurent Daniel, Ahmed Loukili

▶ **To cite this version:**

Laurent Daniel, Ahmed Loukili. Behavior of High Strength Fiber-Reinforced Concrete beams under cyclic loading. Structural Journal, 2002, 99 (3), pp.248-256. 10.14359/11908 . hal-01005287

HAL Id: hal-01005287
https://hal.science/hal-01005287

Submitted on 2 Mar 2017

HAL is a multi-disciplinary open access archive for the deposit and dissemination of scientific research documents, whether they are published or not. The documents may come from teaching and research institutions in France or abroad, or from public or private research centers.

L'archive ouverte pluridisciplinaire **HAL**, est destinée au dépôt et à la diffusion de documents scientifiques de niveau recherche, publiés ou non, émanant des établissements d'enseignement et de recherche français ou étrangers, des laboratoires publics ou privés.

Distributed under a Creative Commons Attribution| 4.0 International License

Behavior of High-Strength Fiber-Reinforced Concrete Beams under Cyclic Loading

by Laurent Daniel and Ahmed Loukili

This study investigated both the influence of longitudinal steel ratio and steel fiber length on high-strength concrete (HSC) beams' behavior under alternate cyclic bending. The evolution in both structural properties and cracking patterns was compared with results from the monotonic bending test. To observe the influence of fibers on deterioration of mechanical properties due to loading cycles, high-strength fiber-reinforced concrete (HSFRC) beams were tested using two fiber lengths: 30 and 60 mm. This analysis highlighted the positive effect of fibers on both the secant structural stiffness and the cracking patterns during the prepeak stage. For the postpeak stage, the ductility measurement did not reveal any improvement. In seismic cases, however, the measurement of cyclic dissipated energy is an important parameter in evaluating structural behavior. Within this framework, the positive effect of fibers on energy dissipation as well as on the cumulative damage capacity has been underscored.

Keywords: crack; fiber-reinforced concrete; high-strength concrete.

INTRODUCTION

It is well-known that high-strength concrete (HSC) is a material featuring many favorable aspects, not only by virtue of its high compressive strength, but also through its durability improvements. The mechanical tests in the literature, however, have revealed the brittleness of HSC and the low rate of increase in tensile strength.[1,2] These features reduced the use of HSC in earthquake zones as a result of recommendations emphasizing the importance of obtaining a ductile material.[3] It is important, however, to mention that, in the case of a high-strength reinforced concrete beam, the structural ductility[4] of HSC can be similar to or better than that of ordinary reinforced concrete beams if the failure mode occurs by steel failure. During an earthquake, however, structures are subjected to reverse loads, which induce both severe tensile damage of concrete and bond deterioration. Hence, the postpeak behavior is particularly influenced by the tensile and bond strength of the concrete.[5]

Previous investigations have shown the effectiveness of fibers on the cracking propagation.[6,7] The greatest improvement involved the increase of dissipated energy, characterized by the uniaxial compressive or tensile behavior of a softened postpeak slope.[8] This focus has served to guide certain studies on structural applications and has pointed out the effectiveness of fibers on cracking control and on shear and bending capacities.[9] The influence of fibers on the structural failure mode, however, depends on a structure's dimension, fiber type, and concrete. Experimental results such as those reported by Espion, Devillers, and Halleux[10] indicated the inefficiency of fibers in ductility increase, and can be opposed to the results given by Chunxiang and Patnaikuni[11] that revealed the good influence of fibers in ductility. These controversial results pointed out the qualified use of fibers under monotonic load, but few papers deal with the influence of fibers on structural behavior under cyclic load.

Table 1—Concrete mixture proportions

Components, kg/m^3	High-strength concrete	High-strength fiber-reinforced concrete
Cement	400	400
Silica fume	40	40
Filler	72.2	69
Sand, 0 to 5 mm	722	690
Gravels, 6 to 10 mm	1010	966
High-range water-reducing admixture	6	10
Water	140	134
Fibers	0	79

The purpose of this paper is to examine the influence of fibers on cyclic beam-bending behavior (cyclic test). Two lengths of fibers are used: 30 and 60 mm. As a tradeoff between loss of workability and increase in structural strength, a reasonable level of steel fibers was chosen: 1% (by volume). To remain close to the structural dimensions used in civil engineering practice, a beam length of 2.75 m (0.11 ft) and a cross section of 150 x 300 mm (6 x 12 in.) are used. The influence of tensile reinforcement is studied by including three different values for the tensile reinforcement ratio ρ.

RESEARCH SIGNIFICANCE

This study reports useful data on the application of high-strength fiber-reinforced concrete (HSFRC) in a seismically active zone. It has been shown that reverse loads involve severe bond deterioration. The control of macrocracks by fibers enhances not only the mechanical properties of high-strength concrete in tension and compression, but also the structural behavior. According to Lemaitre and Chaboche,[12] mechanical properties of HSFRC, such as strength and ductility, are strongly influenced by length of fibers; consequently, this work brings some information about structural behavior enhancement by fibers with respect to both the length of fibers and to the longitudinal reinforcement ratio used. These results broaden the application of fibers to reinforced concrete structures in seismically active zones.

MATERIAL PROPERTIES

Three types of concrete were used for the purposes of this study: HSC, HSFRC with a fiber length of 30 mm ($HSFRC_{30}$), and HSFRC with a fiber length of 60 mm ($HSFRC_{60}$). The mixture components for these concretes are given in Table 1.

Laurent Daniel *is a postgraduate student from the Laboratoire de Génie Civil de Nantes St-Nazaire, Ecole Centrale de Nantes, Nantes, France. His research interests include the mechanical improvement of new concrete (high-strength concrete and high-strength fiber-reinforced concrete) and its structural application under severe environmental and loading conditions.*

ACI member **Ahmed Loukili** *is an assistant professor in the Laboratoire de Génie Civil de Nantes St-Nazaire, Ecole Centrale de Nantes, from which he received his PhD in 1996. His research interests include the early-age properties of concrete, shrinkage, creep and shrinkage, and structural mechanics of high-strength concrete.*

A portland cement with low C_3A content was used. Undensified silica fume was added at a proportion of 10% of cement mass. The water-binder ratio was 0.32. To avoid a loss of workability due to the inclusion of fibers, the quantity of high-range water-reducing admixture was adjusted from 0.54 to 1% dry extract of cement mass The fibers were hook-ended to enhance the anchorage in the matrix. The length diameter ratio of the fibers l/d_f served as an efficiency factor,[4] and the optimum value used in the fibers' reinforced concrete production is $l/d_f = 80$. This ratio has therefore been chosen for the two types of fibers. The fiber volume was constant at 1%. Fiber characteristics are displayed in Table 2.

Compressive tests were carried out on 110 x 220 mm (4.3 x 8.6 in.) cylindrical specimens after 28 days using a testing machine under load control at a loading rate of 0.5 MPa/s. The concrete specimens were kept at 20 °C and 95% relative humidity during the setting process, and then demolded 24 h after casting. Compressive tests were performed on three specimens for each type of concrete, and results are presented in Table 3. The compressive strength of HSC was approximately 95 MPa (13.8 ksi), with a strain at peak of 2.4‰. The fibers accounted for a 15% increase in compressive strength, with an average value of 112 MPa (16.2 ksi) for $HSFRC_{30}$ and 118 MPa (17.1 ksi) for $HSFRC_{60}$. The strain at peak was also increased since it reached 3.1‰ for $HSFRC_{30}$ and 2.7‰ for $HSFRC_{60}$, and highlighted the ability of HSFRC to store a higher quantity of energy in the prepeak domain than HSC.

EXPERIMENTAL PROGRAM

The general test setup and beam cross section are described in Fig. 1(a). A dynamic actuator was used to apply reverse loads on beams 2.75 m in length and 150 x 300 mm in cross section. A positive and negative loading direction was introduced by means of a threaded rod system linked to the beam. The span-depth ratio *a/d* was chosen to obtain bending failure. To generate failure between the loading points, stirrups (diameter of 8 mm, spacing of 20 cm) were arranged outside the pure bending zone. The influence of the reinforcement on beam behavior was analyzed by testing three different values for the tensile reinforcement ratio (0.55, 0.97 and 1.52%) using longitudinal bars 12, 16, and 20 mm in diameter, respectively. The steel was Type FeE500 (tensile yield strength: 500 MPa).

Each support was fitted with a swiveling frame that prevented vertical displacement but allowed rotation about the *z*-axis (Fig. 1(b)). The horizontal displacement was introduced by rollers arranged on one of the supports.

The cyclic tests were displacement controlled. A 0.5 Hz loading frequency was selected to reach the ultimate state of the beams. To measure strength deterioration at a given amplitude deflection, the loading sequence (Fig. 2) was adjusted to 30 s. All of the test features related to the beams are given in Table 3.

Table 2—Hooked-end steel fiber features

Length L_f, mm	Diameter D_f, mm	Aspect ratio L_f/D_f	Shape	Tensile strength, MPa	Modulus of elasticity, GPa
30	0.38	79		2000	200
60	0.75	80		2000	200

Table 3—Details of beam series

Beam type	Steel ratio ρ, ϕ mm	Loading	Concrete	f_c, MPa
L-ref	0.55% (12 mm)	Cyclic	HSC	97
L-30			$HSFRC_{30}$	110
L-60			$HSFRC_{60}$	116
M-ref	0.97% (16 mm)	Static	HSC	91
		Cyclic	HSC	95
M-30			$HSFRC_{30}$	112
M-60			$HSFRC_{60}$	117
H-ref	1.52% (20 mm)	Monotonic	HSC	97
		Cyclic	HSC	94
H-30			$HSFRC_{30}$	114
H-60			$HSFRC_{60}$	117

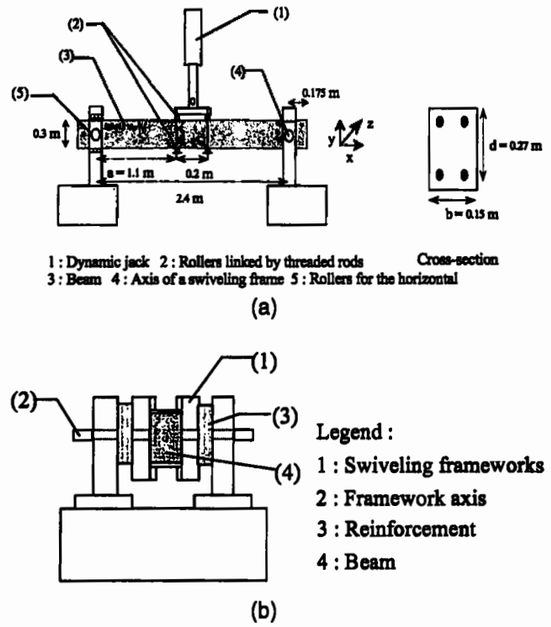

Fig. 1—(a) Testing setup and beam cross section; and (b) alternate bending supports.

BOND DETERIORATION UNDER REVERSE LOADS

A cyclic loading is the worst case of loading, as each concrete layer is alternately submitted to tension and compression stresses. Concrete and steel-concrete bonds are severely damaged. The bond deterioration mechanism observed by Popov[13] is described in Fig. 3(a) to (d) and relates to the typical cyclic load deflection curve presented in Fig. 4, which displays the following:

- Before the peak load: During the positive loading (Fig. 3(a)), the difference between the steel and concrete Young's moduli generates bond stresses. Once the limit tensile stress of the concrete has been reached, cracks

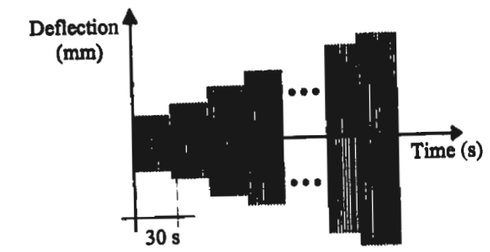

Fig. 2—Loading sequence.

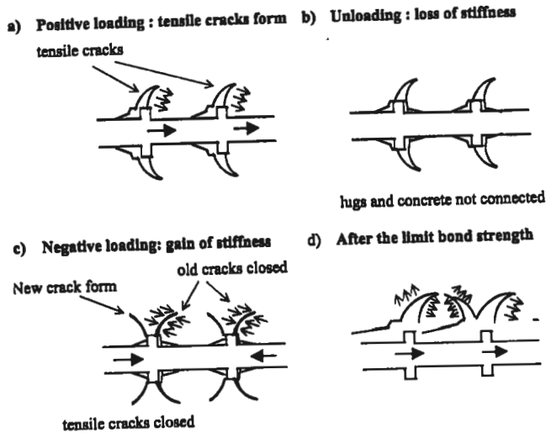

Fig. 3—Bond deterioration mechanism.

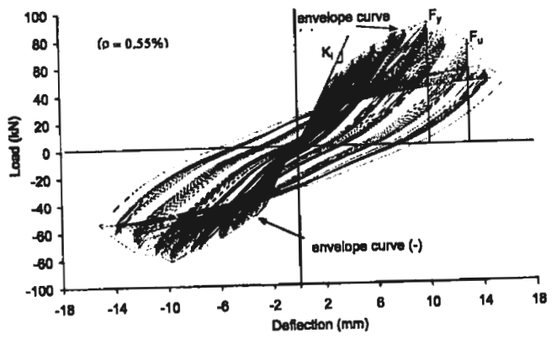

Fig. 4—Typical cyclic curve and envelope curve ($HSFRC_{30}$ beam).

occur and low anelastic strain remains (Fig. 3(a)). During unloading, the secant structural stiffness K on the load-deflection curve is regulated both by the strain of tensile bars and by the strain of the compressive zone. Once the load is close to zero, lugs and concrete are no longer connected, and compressive forces are used to close the tensile cracks (Fig. 3(b)). This mechanism involves a decrease in secant structural stiffness up until the closure of the tensile cracks and the connection between lugs and concrete (Fig. 3(c)). The secant stiffness can then be increased and new cracks generated due to compressive stresses of the bars, which may explain the pinching of the curves during the loading phases; and

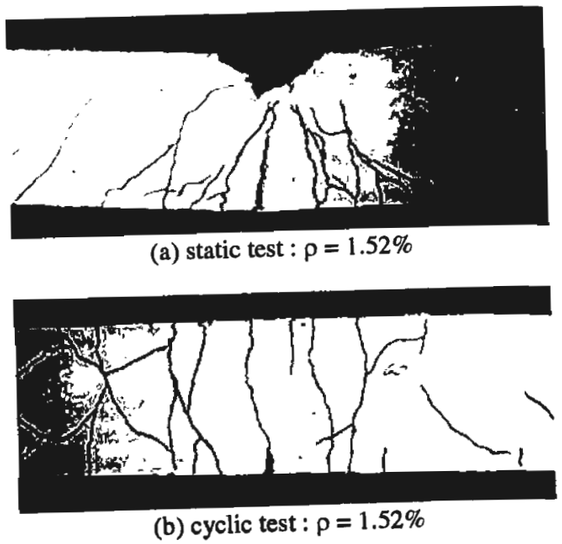

(a) static test : ρ = 1.52%

(b) cyclic test : ρ = 1.52%

Fig. 5—Cracking pattern of HSC beams under cyclic and monotonic loading.

- After the peak load: Bond deterioration is severe (Fig. 3(d)), and the residual steel strain is very high. Consequently, during a reverse load, the tensile steel strain remains and prevents the closure of previous tensile cracks. The secant stiffness cannot be increased, and the pinching disappears (Fig. 4).

COMPARISON BETWEEN MONOTONIC AND CYCLIC TESTS

To measure the influence of reverse loads on structural properties, two static tests were carried out on HSC beams with ρ = 0.97% and ρ = 1.52%, respectively. The analysis focused on both the cracking pattern and the load-deflection curves.

Cracking pattern

The expansion of the cracking zone can be observed in Fig. 5(a) and (b). The reverse loads prevent the concrete from crushing, but the cracks propagate throughout the depth over a wider zone. Moreover, a greater number of horizontal cracks are located at the level of the steel bars, thereby demonstrating the severity of steel-concrete bond deterioration.

The minimal and maximal spacings measured in static tests are close to those obtained by Maurel[14] on beams with a similar cross section and a shear span of 0.8 m (minimal spacing of 5 cm and maximal spacing of 12.5 cm). The longitudinal steel ratio seems to have little influence on the spacing of cracks. The cyclic tests, however, show an increase in the spacing of cracks within the shear zone, and thus, an increase in maximal spacing. This finding can be explained by the different stages of the cracking process. At first, bending cracks occur with low structural damage, and a similar cracking development to static test is denoted. Afterwards, under alternate loads, steel-concrete debonding reduces the rate of occurrence of transverse cracks while inducing horizontal cracking.

Load-deflection curves

As a means of comparing tests under monotonic and cyclic loads, average envelope curves have been used in the cyclic

Table 4—Effect of loading type on mechanical properties

			Monotonic loading				Cyclic loading			
ρ, %	Load level		Load, kN	Deflection, mm	K, kN/mm	μ_δ	Load, kN	Deflection, mm	K, kN/mm	μ_δ
0.97	A	—	27.9	1.3	21.1	—	32.0	1.4	22.9	—
	B	F_{max}	102.0	18.0	5.7	—	91.6	10.3	8.9	—
	C	-15% F_{max}	86.5	43.0	2.0	2.38	76.6	15.6	4.9	1.52
1.52	A	—	29.2	1.9	15.6	—	30.9	2.0	15.1	—
	B	F_{max}	166.8	17.6	9.5	—	152.9	15.1	10.1	—
	C	-15% F_{max}	—	—	—	—	130.0	18.3	7.1	1.22

Note: μ_δ = ductility for 15% load drop.

cases. One example of such an envelope curve is drawn in Fig. 4. A comparison of different curves is provided in Fig. 6, and some mechanical properties are given in Table 4.

Before the peak load, it has been noted that alternate loading does not change the secant stiffness of the HSC beams, but does induce a decrease in maximal load capacity by approximately 10%.

Beyond the peak load, the slope of the cyclic curve drops sharply and accounts for the decrease in structural ductility. This ductility is defined as the ratio of ultimate deflection to the deflection at the peak load δ_u/δ_{Fmax}. A study of this structural ductility was the topic of another paper.[15] The ultimate deflection corresponds to the deflection measured at 85% of the peak load. For ρ = 0.97%, the cyclic loading decreases the ductility by 36%. For ρ = 1.52%, data acquisition was not performed beyond the postpeak, but it was thought that the loss in ductility would not be so high as a result of the greater brittleness of beams exhibited by the increase of tensile reinforcement under monotonic loading. Cracking degrades the steel-concrete bond. As long as the anchorage of bars and the force redistribution in the compressive zone are effective, the structural behavior remains similar. Under alternate stresses, both the cyclic softening of materials[12] and the time lag of the force redistribution in the compressive zone due to crack closure lead to a steep postpeak branch.

INFLUENCE OF FIBERS ON CYCLIC BEHAVIOR

The structural tests with fiber reinforced concrete (FRC) have demonstrated the influence of the steel reinforcement ratio on fiber efficiency.[16] For this reason, three values of the longitudinal steel ratio have been used: ρ = 0.55, 0.97, and 1.52%. Both the concentration and the *l/d* ratio of fibers are also used as efficiency factors. It has therefore been decided to use a constant fiber volume of 1% with an *l/d* ratio of 80. It should be pointed out that the size of the structure is another important factor in regard to the structural efficiency of the FRC; however, the size effect has not been raised herein since all beam specimens have the same height. In this paper, the influence of fibers has focused on the cracking pattern, strength deterioration, the load-deflection envelope curves, and the cumulative damage capacity.

Influence on apparent cracking

The influence of fibers on the apparent cracks can be visualized in Fig. 7(a) to (c), which have been extracted from the M-series (ρ = 0.97%) after the beams' failure.

Between loading points—Figure 7(a) shows a fine and straight main crack for HSC beams, while it is wider and

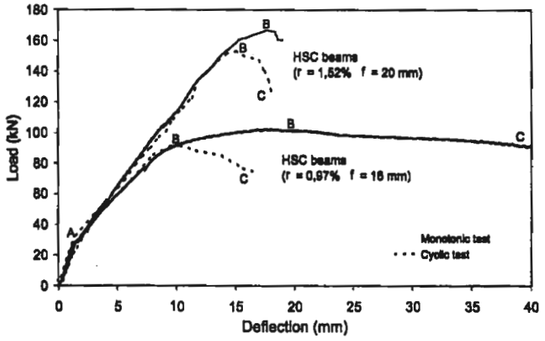

Fig. 6—Static and cyclic tests on HSC beams.

more sinuous when fibers are added (Fig. 7(b) and (c)). It is important to note that this observation is made at the end of test. Indeed, if fibers are often used to reduce the crack width during service loads, their bridge effect allows an increase of the main crack width during the failure stage. The measure of the crack width, however, was not recorded due to the difficulties induced by both alternated loads and continuous measurement.

For the M-30 test, fibers induce a multicracking on the upper part of the beam. At the loading points, bending cracks propagate throughout the beam height for both the L-ref and M-ref series; with the long fibers, however, some bending cracks appeared but did not connect one to the other.

Outside loading points—The HSC beams display some characteristic shear and horizontal cracking, which reveals the deterioration of the steel-concrete bond (Fig. 7(a)). With the addition of fibers, both the number and length of cracks are reduced (Fig. 7(b) and (c)). The shear cracks seem to be effectively bridged by the fibers. Moreover, the horizontal cracks are not located on the HSFRC beams and reflect the action of fibers on cracking induced by steel-concrete debonding. Some isolated cracks can be noted, however, which suggests the random bridging effect of fibers inside the cross sections.

Influence on load-deflection envelope curves

Figure 8 presents cyclic envelope curves that resulted by taking an average of positive and negative envelope curves. The deflection gain at the peak load is insignificant; the curves were thus drawn with respect to a normalized deflection relative to the peak deflection, and correspond to the definition of structural ductility. Three stages can be distinguished: the first is a structural behavior without any damage, as char-

Table 5—Results of tested beams

	Vol. of fibers, %	f_{c28}, MPa	F_1, kN	K_I, kN/mm	F_{max}, kN	δ_{Fmax}, mm	K_{Fmax}	μ_δ[1]
L-ref	0	97	24	18.8	58.5	9.2	6.3	1.52
L-30	1	110	46	20.1	85.8	9.9	8.6	1.31
L-60	1	113	62	20.5	93.1	9.9	9.4	1.28
M-ref	0	95	38	19.4	89.0	10.3	8.6	1.40
M-30	1	112	47	20.9	115.6	11.0	10.5	1.22
M-60	1	115	62	23.4	124.2	12.1	10.3	1.20
H-ref	0	94	38	18.2	151.1	15.1	10.0	1.20
H-30	1	114	40	18.6	159.2	13.7	11.6	1.20
H-60	1	116	68	18.9	178.5	15.0	11.9	1.18

Notes: $f_{c_{28}}$ = compressive strength of concrete at 28 days; F_1 = first cracking load; K_I = initial secant stiffness; and $K_{F_{max}}$ = secant stiffness at peak load.

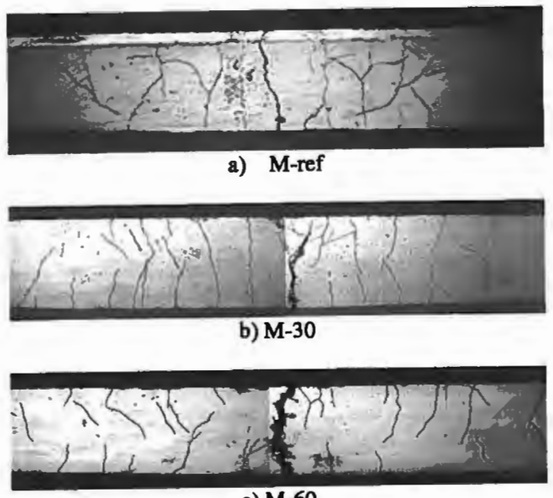

a) M-ref

b) M-30

c) M-60

Fig. 7—Bending and shear cracks on M-series.

acterized by the secant initial stiffness K_I and the first cracking load F_1; the second stage is the damaged behavior up until the maximal load applied with a decreasing secant stiffness; and the last stage is the postpeak behavior that induces structural collapse. The specific values measured off of the curves are listed in Table 5.

Undamaged behavior (prepeak)—The initial secant stiffness, as shown in Table 5, is hardly increased by the presence of fibers; no real difference between $HSFRC_{30}$ and $HSFRC_{60}$ can be observed. The beam's behavior is still elastic, it seems that only microcracking occurs inside the matrix. To enhance this initial stiffness, fibers would have to bridge these microcracks; consequently, the length of fibers needs to be shorter[17] (maximal length: 13 mm). With the length of fibers used in this work (that is, 30 and 60 mm), only macrocracks are bridged as the result of the improvements brought during material testing (increased strength and ductility of HSC).

When either the upper or lower concrete layer of the beam reaches the tensile stress limit, a macrocrack occurs. Should this crack not be bridged by the fibers, the tensile stress would suddenly be distributed in the tensile steel bars, and the secant structural stiffness of the beam would decrease. With HSFRC, as fiber length increases, the value of F_1 also increases. This improvement is particularly distinct at the

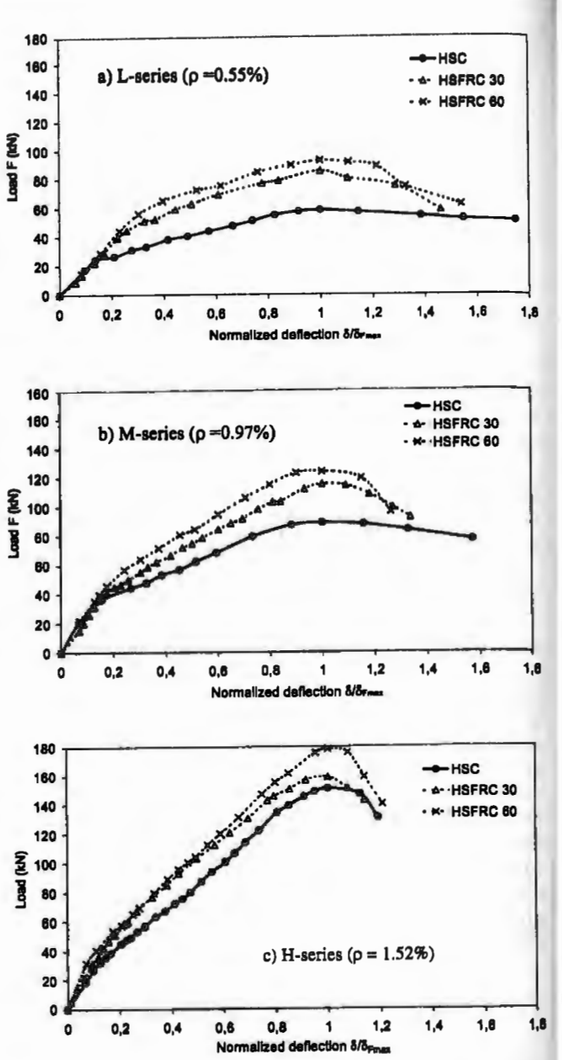

Fig. 8—Load-deflection envelope curves on L-, M-, and H-series.

low reinforcement ratio (ρ = 0.55%) since F_1 increases by 77% with $HSFRC_{30}$ and by 170% with $HSFRC_{60}$. This finding highlights the efficiency of fibers to delay the macrocracks' propagation. Due to the secant stiffness being controlled by the tensile bars, however, the value of F_1 rises less rapidly when the reinforcement ratio increases.

Damaged behavior (prepeak)—In this stage, bending and shear cracks occur and propagate but also bond cracks, as detailed previously. The bridging of cracks by fibers induces an increase in secant stiffness, accentuated by the length of the fibers. This improvement is effective throughout the loading stage up to the peak load. The yielding of reinforcement occurs prior to the peak, but no significant change of stiffness is observed. Table 5 displays an increase in the peak load of HSFRC compared with that of HSC by 47, 30, and 5% for the L-30, M-30, and H-30 tests, respectively, and an increase of 59, 40, and 18% for the L-60, M-60, and H-60 tests. It can be noted that the increase in the tensile bar ratio reduces the gain contributed by the fibers, due to a wider crack opening

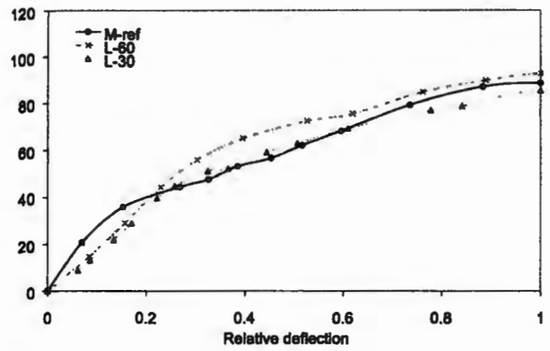

Fig. 9—Fibers replacing reinforcement capacity (comparison of L-30, L-60, and M-ref).

for higher reinforcement ratio. Studies focusing on the steel-concrete bond with HSC[18] have indeed shown that the crack opening is related to the steel bar diameter. For the H-30 test, the crack opening at the peak load seems to be too wide for the 30 mm fibers, which explains the negligible gain. Nevertheless, by preventing against the propagation of cracks, both $HSFRC_{30}$ and $HSFRC_{60}$ contribute to the increase in secant stiffness and thereby to the slowing rate of beam damage.

At this point, it is worth mentioning that for low longitudinal reinforcement ratios, fibers can replace some of the longitudinal bars (Fig. 9). This is important since this phenomenon has not been observed with big dimension beams under monotonic bending loads.[10] Only the replacement of stirrups with fibers has been foreseen according to certain studies.[7,11]

Collapse behavior (postpeak)—Many of the codes used to investigate structural performance during the failure stage are based on ductility measurements. Ductility has been defined as the ratio of the ultimate deflection to the deflection at the peak load (δ_u/δ_{Fmax}). In this paper, the ultimate deflection is assessed when the beam supports just 85% of the maximal load. This definition is based on the work of Park and Ang[19] that was then modified by Srinivas et al.,[20] who considered that under cyclic and alternate loading, structures were too heavily damaged beyond this level of loading capacity. In Table 5, the ductility measurement indicates the inefficiency of the fibers. For each series, the concrete is severely degraded by tensile stresses at peak, and the maximal load gain obtained by fibers actually induces a drop in ductility due to a severe bond deterioration between reinforcement bars and concrete. Considering a support capacity of 95% of F_{max}, the analysis conducted by Daniel and Loukili[21] indicates a similar ductility obtained with $HSFRC_{60}$ relative to HSC for the L-series and relative to $HSFRC_{30}$ for the M-series. This finding underscores the influence of long fibers with a low reinforcement ratio; however, the improvement is not substantial enough, and the small sample size only indicates some trends. More exploration should be realized to recommend the use of fibers for structural ductility-enhancement requests.

Influence on cumulative dissipated energy

Measuring ductility is not the only motivation for investigating behavior during the postpeak phase. When earthquakes occur, energy gets injected into the structure and then has to be dissipated for safety reasons. According to this setup, the behavior of fibers inside the matrix acts as a dissipative mechanism. The measurement of dissipated energy could thus become a good efficiency index independently from structural ductility considerations.

During cyclic tests on structures, dissipative mechanisms are frequently encountered and must be distinguished to determine the action of fibers on the dissipated energy (Eq. (1)). In fact, a principal energy E_T is injected into the structure, composed of a beam or column and supports. One component of this energy is redistributed into the soil E_s, while the other is used by the structure over the elastic E_e and inelastic E_a domains.[1] The first component E_e represents the energy necessary both for beam displacement (kinematics energy E_c) and for elastic strain E_{es}. The latter component E_a includes damping energy and hysteretic energy

elastic domain inelastic domain

$$E_T - E_s = \underbrace{E_c}_{E_c + E_{es}} + \underbrace{E_a}_{E_d + E_h} \quad (1)$$

Structural collapse corresponds herein to the case observed when the structure is no longer able to dissipate the accumulated energy.[3] It is therefore important to increase the energy storage capability in the elastic domain and the energy dissipation in the inelastic domain. For the first aforementioned point, the use of HSC increases structural stiffness due to the contribution of high compressive strength as well as to the improvement of the steel-concrete bond. The low tensile strength and brittle nature of concrete, however, prevent the possibility of increasing energy in the inelastic domain. Adding fibers inside the high-strength matrix limits concrete damage in the elastic domain, and results in energy dissipation in the inelastic domain due to the strain and fiber slip inside the matrix.

The dissipated energy during a loading cycle was determined by computing the hysteretic area of the loop. The increase of dissipated energy during cycles at similar displacement amplitudes is low. It was thereby assumed that the contribution of fibers is concentrated during the first cycle of each displacement amplitude. The computation of primary dissipated energy was carried out up until total collapse (Fig. 10).

For L-series—Fibers increase the dissipation of energy up until collapse. The gain provided by the longest fibers, compared with the shorter ones, is observed at the end of the test for a normalized deflection of greater than 1.4. The maximal dissipated energy increases by 45% for $HSFRC_{60}$ (1490 kNmm) with respect to HSC, while for $HSFRC_{30}$ it increases by only 13%.

For M-series—Only the $HSFRC_{60}$ increases the dissipation of energy up until collapse, with an increase in ultimate dissipation (2240 kNmm) of 41% with respect to HSC. The behavior of $HSFRC_{30}$ is similar to that of HSC, with a low increase in dissipated energy over the postpeak zone. Furthermore, the maximal value is 26% less than HSC, which highlights the low effectiveness of shorter fibers.

For H-series—A reduction in the improvement of long fibers is noted since the maximal energy with respect to HSC increases by 28%. $HSFRC_{30}$ does not show good behavior, as the level of energy dissipation remains less than that of the HSC beam during the entire postpeak stage.

There were not enough repetitive tests to draw firm conclusions, but some trends could be mentioned. It seems that

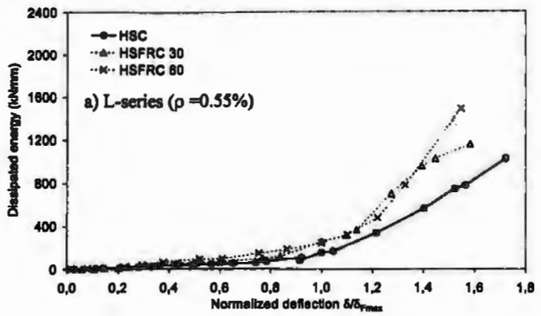

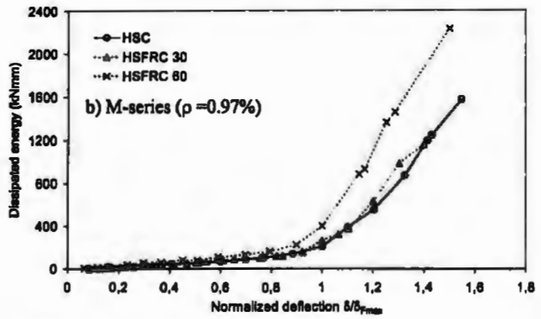

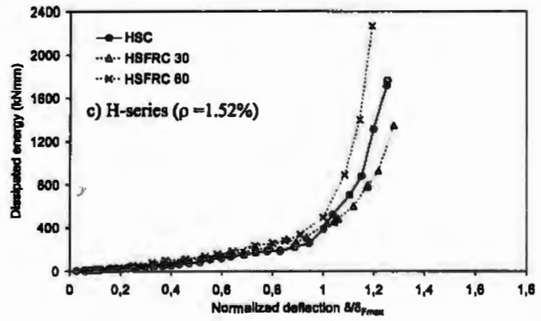

Fig. 10—Dissipated energy versus normalized deflection.

the inclusion of fibers leads to an improvement in energy dissipation, which is particularly efficient at low longitudinal steel reinforcement ratios. As the tensile bar ratio increases, the maximal dissipation rate drops. The postpeak behavior of the $HSFRC_{60}$ beam can be considered as good for all series. Only the L-series, however, exhibits an efficient dissipation of the $HSFRC_{30}$ beam.

STRUCTURAL DAMAGE INDEXES

Many authors have established a set of damage indexes to ascertain the residual capacity of structures. A wide array of parameters may be used, such as number of cycles, stiffness, and ductility. When reverse loads are applied (refer to the previous section), however, the importance of energy dissipation is readily apparent. The energy indicator proposed by Darwin and Nmai[22] provides an assessment of the dissipative capacity compared with the elastic energy injected at peak load. This measurement has been related to the hysteretic area of cycle i, E_i normalized to the elastic energy $F_{max}\,\delta_{F_{max}}$. The iteration on all cycles yields the total normalized cyclic energy (Eq. (2))

$$E_n = \frac{1}{F_{max}\delta_{F_{max}}}\sum_{i=1}^{n} E_i \tag{2}$$

This indicator has been modified by Ehsani and Wright[23] through introducing both the stiffness degradation and the deformation capacity (Eq. (3))

$$D_i = \frac{1}{F_{max}\delta_{F_{max}}}\sum_{i=1}^{n} E_i\left(\frac{K_i}{K_y}\right)\left(\frac{\delta_i}{\delta_y}\right)^2 \tag{3}$$

where

F_{max} = peak load;
$\delta_{F_{max}}$ and δ_i = deflection at the peak and maximal deflection of cycle i, respectively;
E_i = dissipated energy calculated from the area of cycle i; and
$K_{F_{max}}$ and K_i = secant stiffness at the peak load and in cycle i, respectively.

These last two cyclic energy indexes express numerical values without any connection to the ultimate state. Other indexes have therefore been devised to compare the energy dissipated under cyclic conditions with that dissipated under monotonic conditions, with numerical values ranging from 0 to 100% (100% denotes structural failure). Meyer[24] defined an indicator D_Q based on the energy ratios in Eq. (4) and (5)

$$D_Q = D_Q^+ + D_Q^- - D_Q^+ D_Q^- \tag{4}$$

with

$$D_Q^{\pm} = \frac{\Sigma E_{pi}^{\pm} + \Sigma E_{si}^{\pm}}{E_u^{\pm} + \Sigma E_i^{\pm}} \tag{5}$$

where

E_{pi} = energy dissipated during the first half-cycle;
E_{si} = energy dissipated during the second half-cycle;
E_u = maximum energy dissipated under monotonic load; and
$\pm$ = positive or negative deformation.

Sadeghi[25] introduced a fatigue factor (Eq. (6)) to decrease the damage caused by cycles of similar amplitude displacement. The expression for the damage index in the positive/negative phase of displacement is given as follows (Eq. (7))

$$D_Q^{\pm} = \frac{\Sigma E_{pi}^{\pm} + \lambda_i^{\pm}\Sigma E_{si}^{\pm}}{E_u^{\pm}} \tag{6}$$

where

$$\lambda_i^{\pm} = \frac{E_u^{\pm} - \Sigma E_{si}^{\pm}}{E_u^{\pm}} \tag{7}$$

The use of this index is not straightforward for structures subjected to many cycles during the postpeak phase. Moreover, some results must be derived from tests under monotonic loading, which would increase the number of tests required overall. To overcome this constraint, a new damage index (Eq. (8)), based on the expression of Sadeghi's index (Eq. (6)), has been developed. A strain factor α_i (Eq. (9)) is introduced for the dissipated energy of each first cycle E_{pi} to stand for the secant stiffness deterioration with respect to the peak load. The damage induced by successive cycles of similar displacement amplitude is attenuated by a fatigue factor λ_i (Eq. (10)) related to the strength deterioration with respect to the first cycle. The energy summation is normalized by the total amount of energy dissipated by each first cycle ΣE_{pi}. The tensile reinforcement ratio ρ is introduced to take into account the difference in energy behavior with increasing tensile reinforcement. The power number is computed to yield an index value close to that for the HSC beams

$$D_i = \rho^{0.4}\frac{\alpha_I^{0.9}\sum E_{pi} + \lambda_i^{0.9}\sum E_{si}}{\sum E_{pi}} \tag{8}$$

$$\alpha_i = \frac{K_{F_{max}} - K_{pi}}{K_{F_{max}}} \tag{9}$$

$$\lambda_i = \frac{F_{pi} - F_{si}}{F_{pi}} \tag{10}$$

where

$K_{F_{max}}$ = secant stiffness at peak load;
K_{pi} = secant stiffness of primary cycles;
F_{pi} = maximal load of primary cycles; and
F_{si} = maximal load of successive cycles.

The cumulative damage capacity of the beams is computed using the index in Eq. (8); results are shown in Fig. 11(a) to (c). The HSFRC beams reveal two phases: 1) the rate of damage is reduced during the first successive cycles in comparison with the HSC beam, with this distinction being particularly strong for the lower tensile reinforcement; and 2) damage related to the loss of ductility in the beams speeds up. For ρ = 0.55%, however, both $HSFRC_{30}$ and $HSFRC_{60}$ successfully increase the cumulative damage capacity with values of greater than one, yet 60 mm fibers appear to reveal a faster damage growth than the others. For ρ = 0.97%, only the $HSFRC_{60}$ manages to enhance the cumulative damage index with respect to HSC with a value similar to that from the previous test. This finding may suggest that 60 mm fibers are not being used up to their maximal efficiency. For ρ = 1.52%, the HSFRC exhibits no increase in the damage index, which underscores the inefficiency of fibers with the higher longitudinal reinforcement ratio.

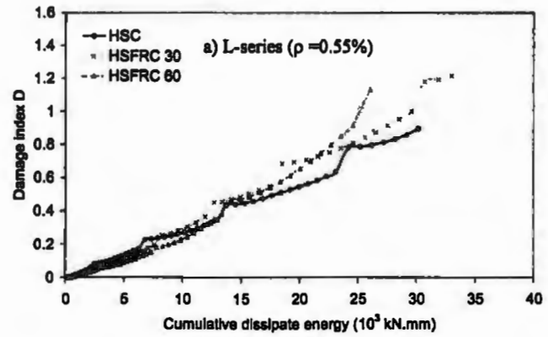

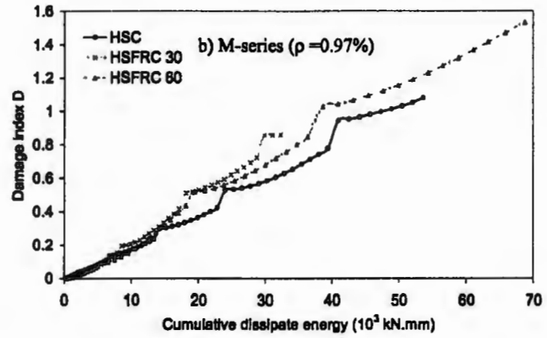

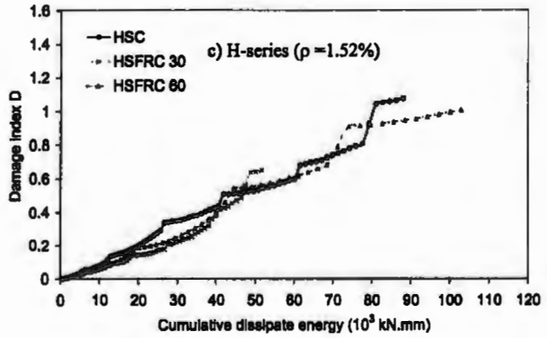

Fig. 11—Damage index D versus cumulative dissipate energy.

CONCLUSIONS

The aim of this study has been to investigate the influence of fibers on the behavior of HSFRC beams under cyclic bending. The severe concrete damage due to alternate loading induces a loss in both maximal load capacity and ductility. This degradation suggests that the use of fibers can be efficient to prevent an early emergence of macrocracks during the prepeak stage. Fibers induce an increase in beam structural stiffness up to the peak load. For a tensile reinforcement ratio of 0.55%, HSFRC exhibits behavior similar to that of an HSC beam with a tensile reinforcement ratio of 0.97%. Nevertheless, the fibers have no influence on strength deterioration during loading cycles at a given displacement. In the postpeak stage, the computation of ductility shows the difficulty involved in improving behavior. The increase in loading capacity of HSFRC beams leads to a steeper slope of the postpeak branch.

Within an energy-based framework, however, and particularly so in the case of earthquake zones, the insertion of long fibers enhances the energy dissipation over both the elastic and inelastic domains for all longitudinal reinforcement ratios; with regard to the 30 mm fibers, however, enhanced energy dissipation only occurs for lower ratios. With respect to energy dissipation alone, however, 30 mm fibers may be recommended for lower reinforcement ratios. The effect on the cumulative damage capacity is positive for 60 mm fibers, with an efficiency limit for ρ = 1.52%. These findings have raised the possibility of using the $HSFRC_{60}$ in small-sized structures (low heights or low reinforcement ratios) in earthquake zones to increase the

mechanical postpeak properties and energy dissipation in the inelastic domain.

NOTATION

D_i = damage index
d_f = fiber diameter
E_i = hysteretic energy of one cycle
F_1 = first cracking load
F_{max} = peak load or maximal load
$K_{F_{max}}$ = secant structural stiffness at peak load
l = fiber length
α_i = strain factor
$\delta_{F_{max}}$ = deflection at peak load
λ_i = fatigue factor
ρ = longitudinal reinforcement ratio

CONVERSION FACTORS

1 mm = 0.039 in.
1 kN = 0.2248 kips
1 MPa = 145 psi

REFERENCES

1. Collins, M. P.; Mitchell, D.; and Gregor, J. G., "Structural Design Considerations for High-Strength Concrete," *Concrete International*, V. 15, No. 5, May 1993, pp. 27-34.

2. Gerard, B.; Marchand, J.; Breysse, D.; and Ammouche, A., "Constitutive Law of High-Strength Concrete under Tensile Strain," *International Symposium on Utilization of High-Strength/High-Performance Concrete*, Paris, 1996, pp. 677-685.

3. Davidovici, V., "Génie parasismique," *Presses de l'Ecole Nationale des Ponts et Chaussées*, Paris, 1985.

4. Mansur, M. A.; Chin, M. S.; and Wee, T. H., "Flexural Behavior of High-Strength Concrete Beams," *ACI Structural Journal*, V. 94, No. 6, Nov.-Dec. 1997, pp. 663-674.

5. Shin, S.-W.; Ghosh, S. K.; and Moreno, J., "Flexural Ductility of Ultra-High-Strength Concrete Members," *ACI Structural Journal*, V. 86, No. 4, July-Aug. 1989, pp. 394-400.

6. Abrishami, H. H., and Mitchell, D., "Influence of Steel Fibers on Tension Stiffening," *ACI Structural Journal*, V. 94, No. 6, Nov.-Dec. 1997, pp. 769-776.

7. Li, Z.; Li, F.; Chang, T.-Y. P.; and Mai, Y.-W., "Uniaxial Tensile Behavior of Concrete Reinforced with Randomly Distributed Short Fibers," *ACI Materials Journal*, V. 95, No. 5, Sept.-Oct. 1998, pp. 564-574.

8. Hsu, L. S., and Hsu, C.-T. T., "Stress-Strain Behavior of Steel-Fiber High-Strength Concrete under Compression," *ACI Structural Journal*, V. 91, No. 4, July-Aug. 1994, pp. 448-457.

9. Casanova, P., "Bétons de fibres métalliques: du matériau à la structure," doctoral dissertation, Ecole Nationale des Ponts et Chaussées, France, 1996.

10. Espion, B.; Devillers, J.; and Halleux, P., "De l'utilisation de fibres métalliques comme armature complémentaire de poutres en béton armé soumises à la flexion," *Materials and Structures*, 1993, No. 26, pp. 479-485.

11. Chunxiang, Q., and Patnaikuni, I., "Properties of High-Strength Steel Fiber-Reinforced Concrete Beams in Bending," *Cement and Concrete Composites*, 1999, pp. 73-81.

12. Lemaitre, J., and Chaboche, J. L., "Mécanique des matériaux solides," Edition Dunod, 1988.

13. Popov, E. P., "Bond and Anchorage of Reinforcing Bars under Cyclic Loading," ACI JOURNAL, *Proceedings* V. 81, No. 4, July-Aug. 1984, pp. 340-349.

14. Maurel, O., "Contribution à l'étude de la fissuration des membrures tendues en béton armé de hautes performances," thesis, Institut National des Sciences Appliquées de Toulouse, France, 1999.

15. Daniel, L.; Loukili A.; and Lamirault, J., "Experimental Behavior of High-Strength Fiber Concrete Beams under Cyclic and Alternated Loadings," *Fifth RILEM Symposium on Fiber-Reinforced Concretes*, Lyon, France, Sept. 13-15, 2000.

16. Kormeling, H. A.; Reinhardt, H. W.; and Shah, S. P., "Static and Fatigue Properties of Concrete Beams Reinforced with Continuous Bars and with Fibers," ACI JOURNAL, *Proceedings* V. 77, No. 1, Jan.-Feb. 1980, pp. 36-43.

17. Rossi, P., "Les bétons de fibres métalliques," *Presses de l'Ecole Nationale des Ponts et Chaussées*, 1998.

18. Hamouine, A., "Contribution à l'étude de l'adhérence acier-béton de hautes performances," thesis, I.N.S.A. de Toulouse, May 1996.

19. Park, Y. J., and Ang, A. H. S., "Mechanistic Seismic Damage Model for Reinforced Concrete," *ASCE Journal of Structural Engineering*, V. 3, 1985, pp. 722-757.

20. Srinivasa Rao, P.; Sivarama Sarma, B.; Lakshmanan, N.; and Stangenberg, F., "Damage Model for Reinforced Concrete Elements under Cyclic Loading," *ACI Materials Journal*, V. 96, No. 6, Nov.-Dec. 1998, pp. 682-690.

21. Daniel, L., and Loukili, A., "Cyclic Bending of High-Strength Fiber Reinforced Concrete Beams: Influence of Fiber Length," *Third International Conference on Concrete under Severe Conditions*, V. 1, Vancouver, Canada, June 18-20, 2001, pp. 843-851.

22. Darwin, D., and Nmai, C. K., "Energy Dissipation of R/C Beams under Cyclic Load," *Journal of Structural Engineering*, ASCE, V. 112, No. 8, Aug. 1986, pp. 1829-1846.

23. Ehsani, M. R., and Wright, J. K., "Confinement Steel Requirements for Connections in Ductile Frames," *ASCE Journal of Structural Engineering*, V. 116, No. 3, 1990, pp. 751-767.

24. Meyer, I. F., "Ein werkstoffgerechtes Schädigungsmodell und Stababschnittselement für Stahlbeton unter zyklisher nichtlinearer Beanspruchung," TR 88-4, RUB, Aug. 1988.

25. Sadeghi, K., "Simulation numérique du comportement de poteaux en béton armé sous cisaillement dévié alterné," thesis, Ecole Centrale de Nantes, France, 1995.